Electronic Supporting Information for:

Highly Efficient Iodine Uptake and Iodate Selective Probe in A 3D Honeycomb–Like Copper–Organic Framework Based On *In Situ* Ligand Transformation

Wen Dai,* Chuanming Zhang, Xiaoang Yang, and Lincai Li

State Key Laboratory of Physical Chemistry of Solid Surface, College of Chemistry and Chemical Engineering, Xiamen University, Xiamen, Fujian 361005, China. E-mail: daiwen95@stu.xmu.edu.cn

Contents

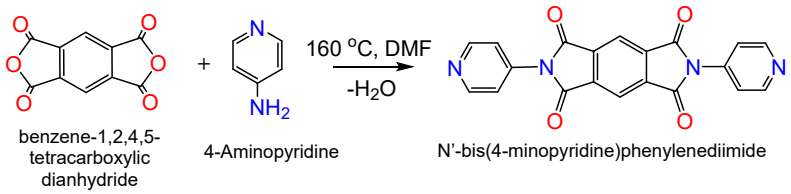

Scheme S1. Synthetic route for N'-bis(4-aminopyridine)phenylenediimide.

Table S1. Crystal data collections and structure refinement parameters for **1**

Compound	**(**CCDC2164832)
Empirical formula	$C_{20}H_{18}N_4O_9Cu$
Formula weight	521.92
Crystal size (mm)	0.15×0.03×0.01
Crystal system	Hexagonal
Space group, Z	$P6_522$, 6
a (Å) ; α (°)	18.8181(8); 90
b (Å) ; β (°)	18.8181(8); 90
c (Å) ; γ (°)	23.6351(7); 120
V (Å^3)	7248.4(7)
ρ_{calcd} (g·cm^{-3})	0.717
μ (mm^{-1})	0.886
F(000)	1602
λ(Cu–$K\alpha$) (Å)	1.54178
T (°K)	150.0(1)
2θ Range (°)	6.588 – 145.466
Collected reflections	18325
Unique reflections	4728
Observed reflections	3860 (>2σ (I))
R_{int}	0.0516
GOF	1.071
Flack parameter	0.14(6)
R indices (for obs.):	
R_1 [a], wR_2[b]	0.0527, 0.1432
R indices (for all):	
R_1, wR_2	0.0649, 0.1527
Largest diff. peak/hole (e.Å^{-3})	0.46/-0.34

[a] $R_1 = \sum(||F_o|-|F_c||)/\sum|F_o|$, $wR_2 = \{\sum w[(F_o^2-F_c^2)^2]/\sum w[(F_o^2)^2]\}^{1/2}$;

[b] $w = 1/[\sigma^2(F_o^2)+(aP)^2+bP]$, where $P = (F_o^2+2F_c^2)/3]$.

Table S2. Selected bond lengths [Å] and angles [°] for **1**.

Cu1-O2a	1.975(3)	Cu1-O1a	2.810(3)
Cu1-O2b	1.975(3)	Cu1-N2	1.985(3)
Cu1-O4	2.351(5)	Cu1-N2c	1.985(3)
O2a-Cu1-O2b	174.9(2)	O2b-Cu1-N2	90.21(13)
O2a-Cu1-O4	92.53(11)	O2b-Cu1-N2c	89.65(13)
O2b-Cu1-O4	92.53(11)	O4-Cu1-N2	91.60(11)
O2a-Cu1-N2	89.65(13)	O4-Cu1-N2c	91.60(11)
O2a-Cu1-N2c	90.21(13)	N2-Cu1-N2c	176.8(2)

Key: a = 1-*y*+*x*, *x*, -1/6+*z*; b = 2-*x*, 1-*x*+*y*, 4/3-*z*; c = 2-*y*, 2-*x*, 7/6-*z*.

Table S3. Comparison of I_2 vapor adsorption in different MOFs materials.

Compound	I_2 adsorption capacity ($mg \cdot g^{-1}$)	Ref.
$Zr_6O_4(OH)_4(peb)_6$	2790	S1
$Zn_2(tptc)(apy)_{2-x}$	2160	S2
CuBTC	1750	S3
$(ZnI_2)_3(tpt)_2$	1730	S4
MFM-300(Sc)	1540	S5
UiO-66-PYDC	1250	S6
ZIF-8	1250	S7
$Ni_4(44pba)_8$	1100	S8
$Cu(INA)_2$	900	S9
TMBP-CuI	750	S10
$Ni(pz)Ni(CN)_4$	590	S11
$Cu_3BTC_2(TIB)_2$	286	S12
$Co_3BTC_2(TIB)_2$	279	S12
SION-8:Ca2(TBAPy)	250	S13
$[Cu(L)(H_2O)]\cdot 2H_2O$	3410	***This work***

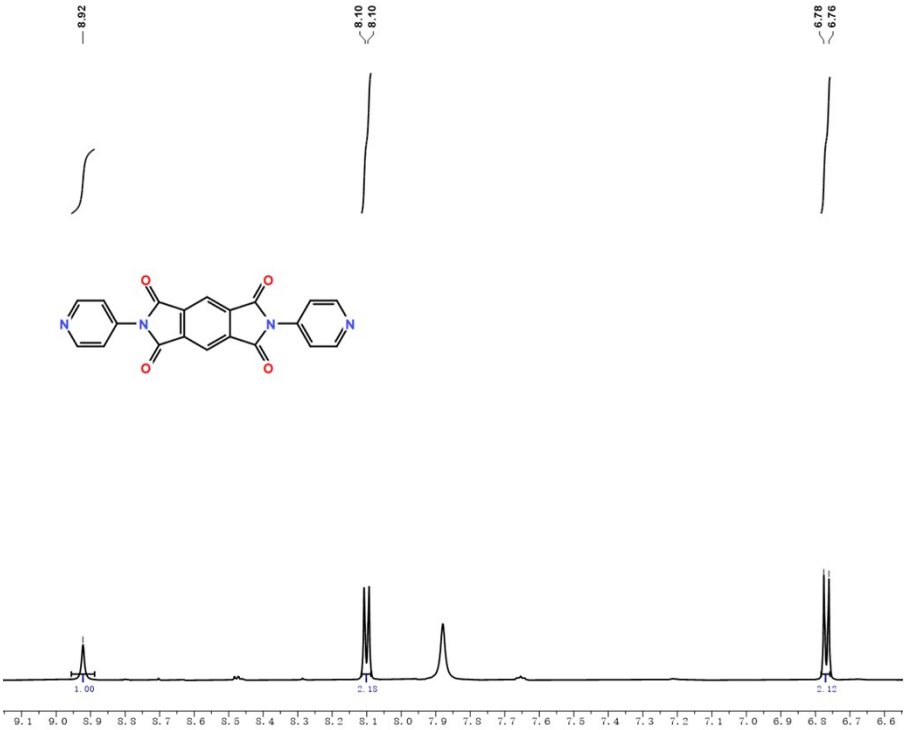

Figure S1. ^{1}H NMR spectra of N'-bis(4-aminopyridine)phenylenediimide in $CDCl_3$ at room temperature.

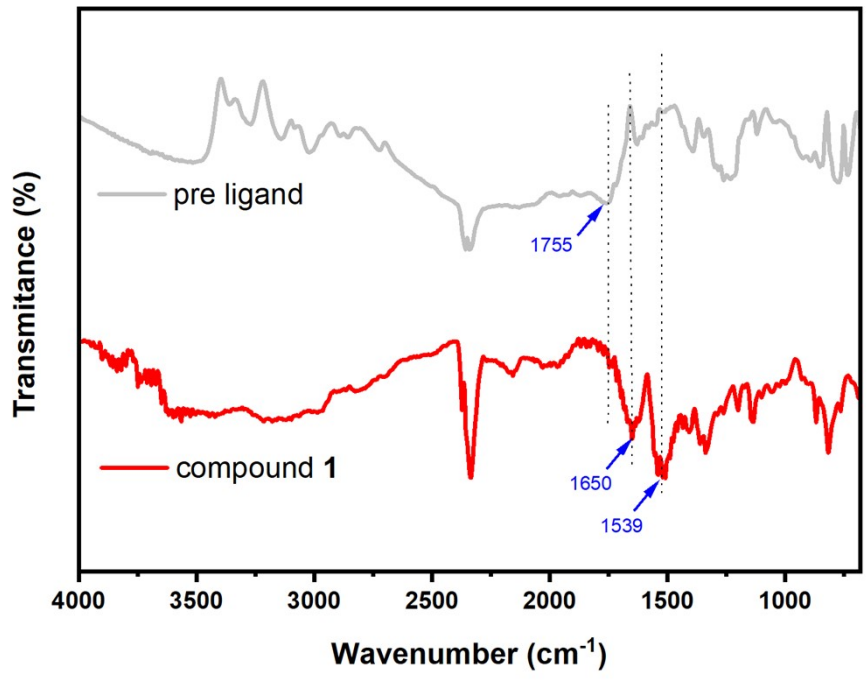

Figure S2. IR spectra for compound **1** *vs* N'-bis(4-aminopyridine)phenylenediimide.

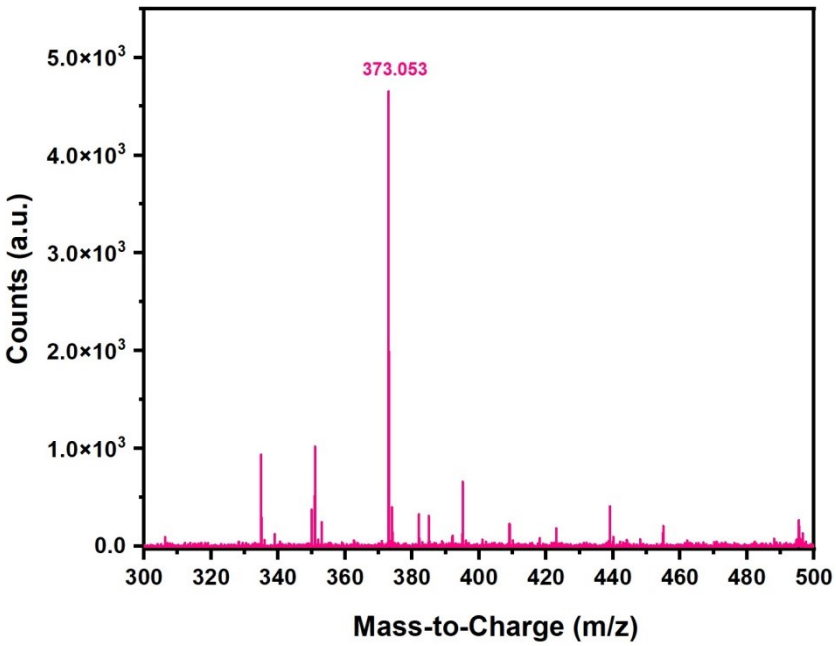

Figure S3. ESI-MS data of N'-bis(4-aminopyridine)phenylenediimide.

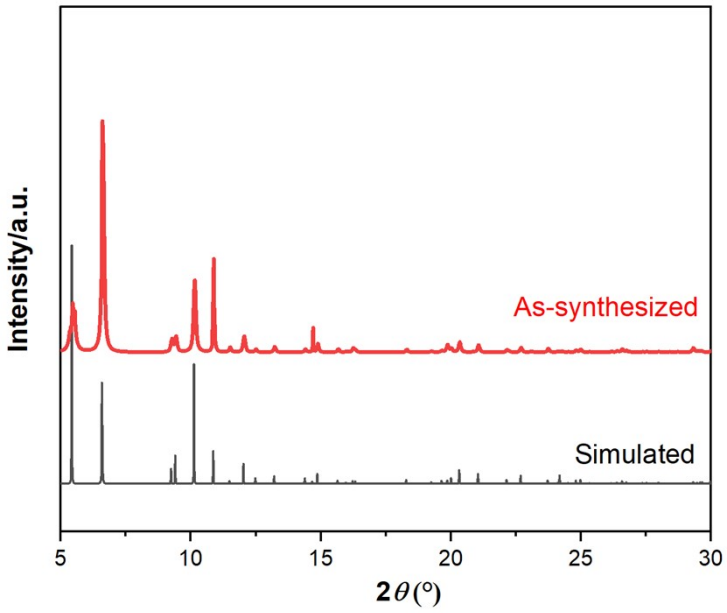

Figure S4. Measured and simulated PXRD patterns of compound **1**.

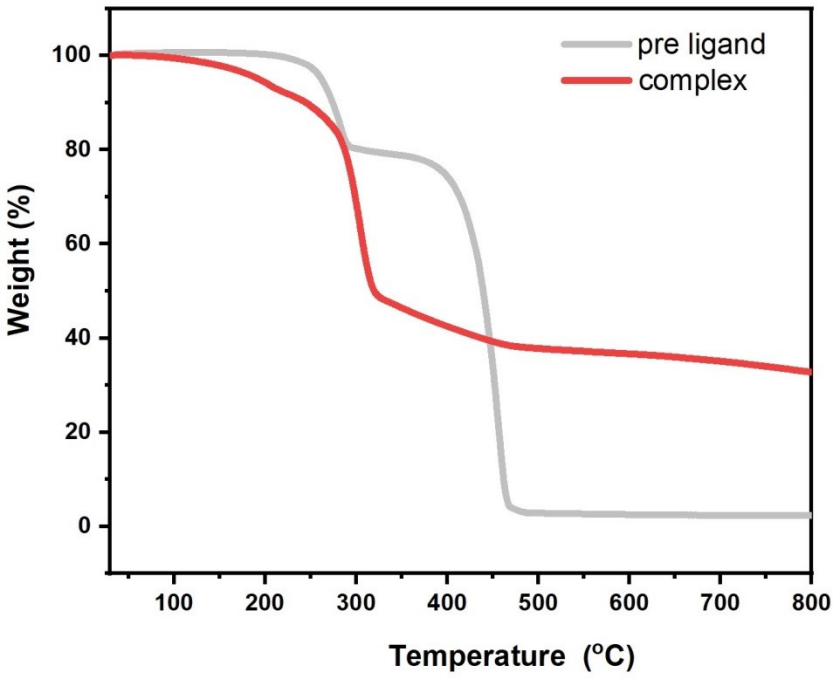

Figure S5. TGA traces of **1** (red line) and N'-bis(4-aminopyridine)phenylenediimide (gray line).

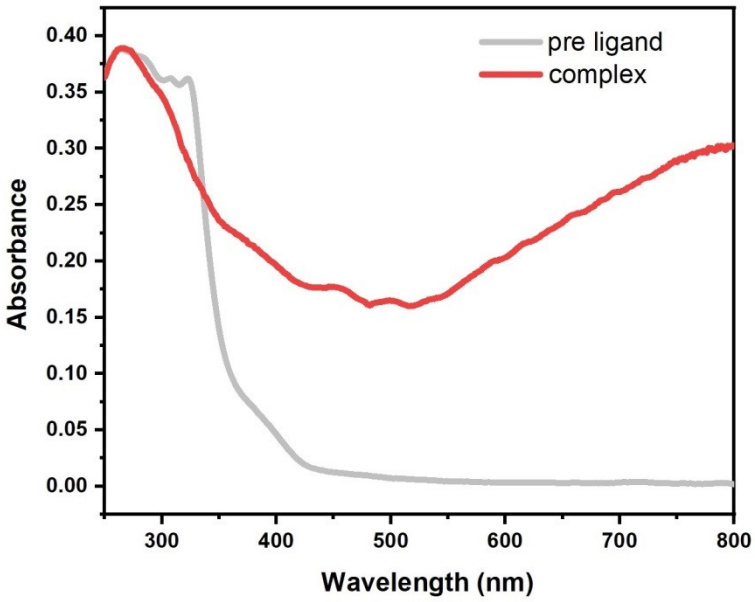

Figure S6. Solid state UV-Vis spectra of compound **1** (red line) and N'-bis(4-aminopyridine)phenylenediimide (gray line).

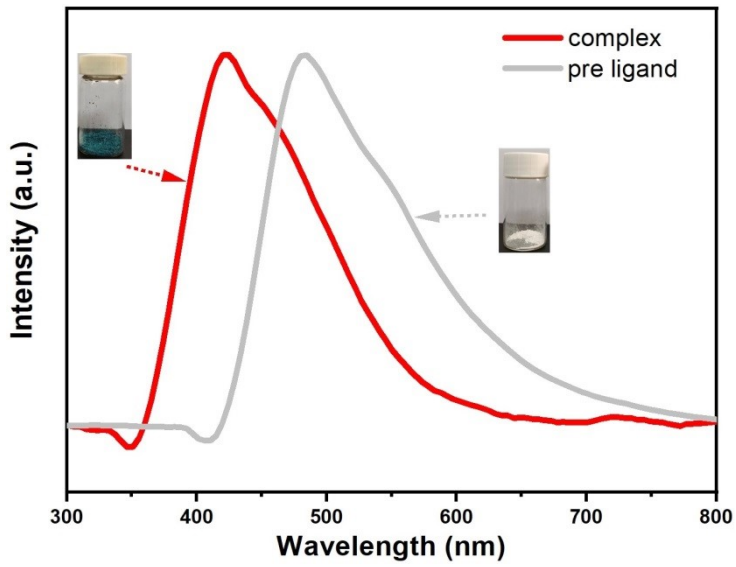

Figure S7. Solid-state fluorescent spectra of compound **1** (red line) and N'-bis(4-aminopyridine)phenylenediimide (gray line).

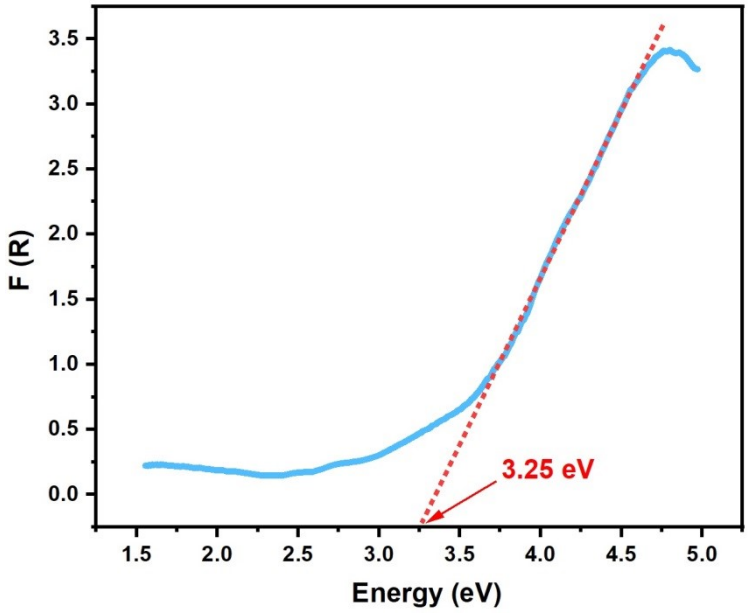

Figure S8. Optical diffuse reflectance spectra of compound **1**.

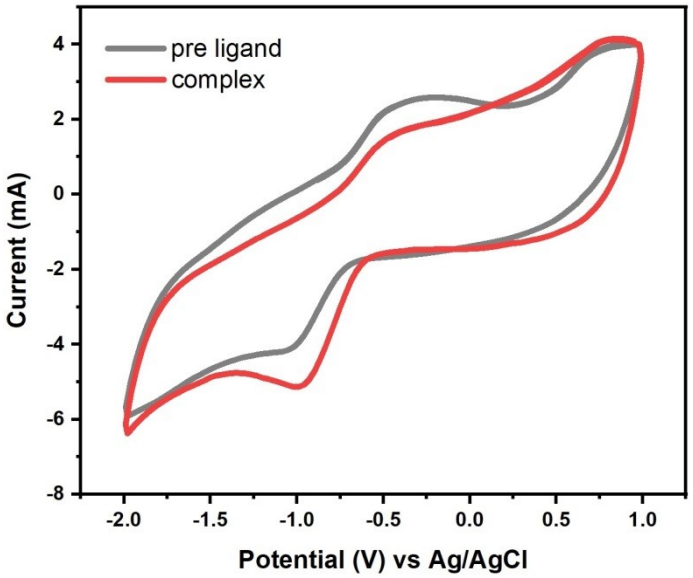

Figure S9. The cyclic voltammograms of compound **1** (red line) and N'-bis(4-aminopyridine)phenylenediimide (gray line).

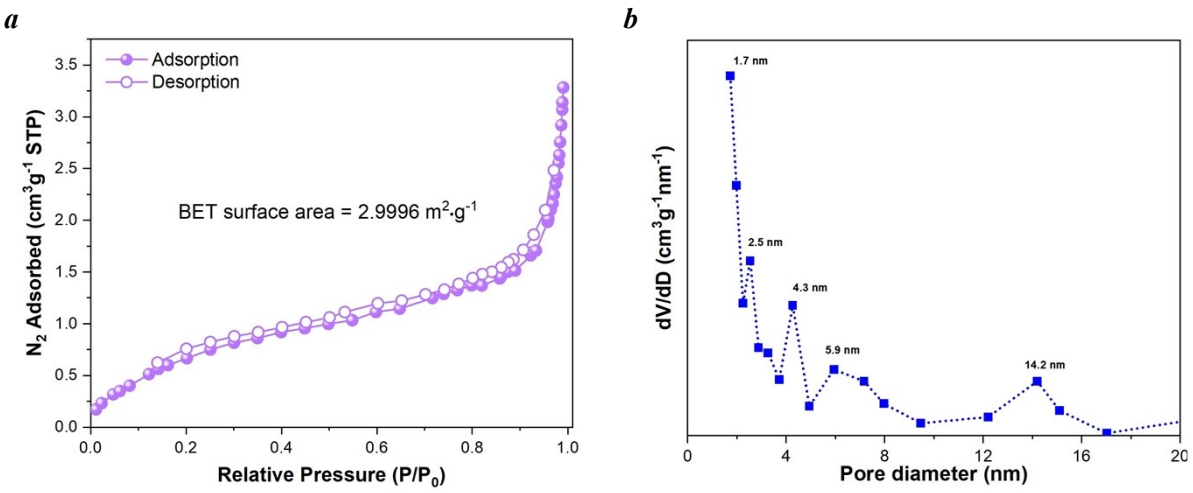

Figure S10. The N_2 adsorption-desorption isotherms (*a*) and porosity feature (*b*) of **1**.

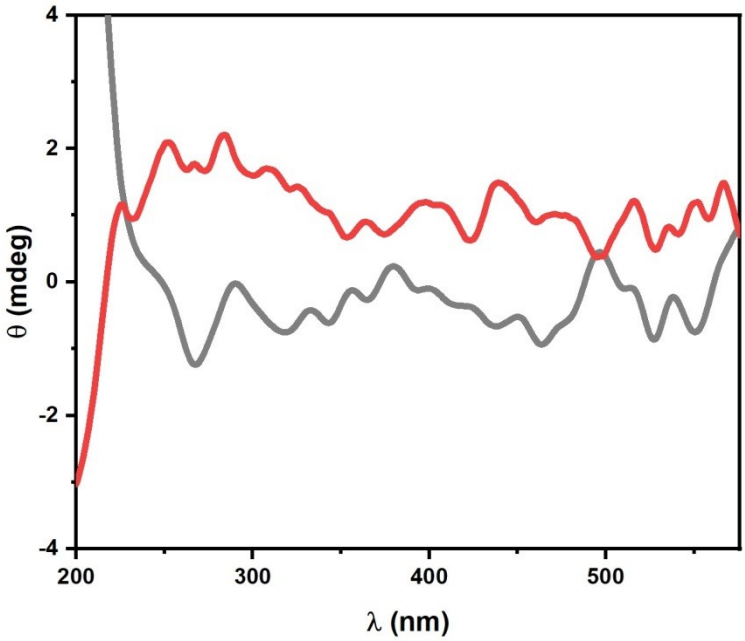

Figure S11. Solid-state circular dichroism spectrum of compound **1**.

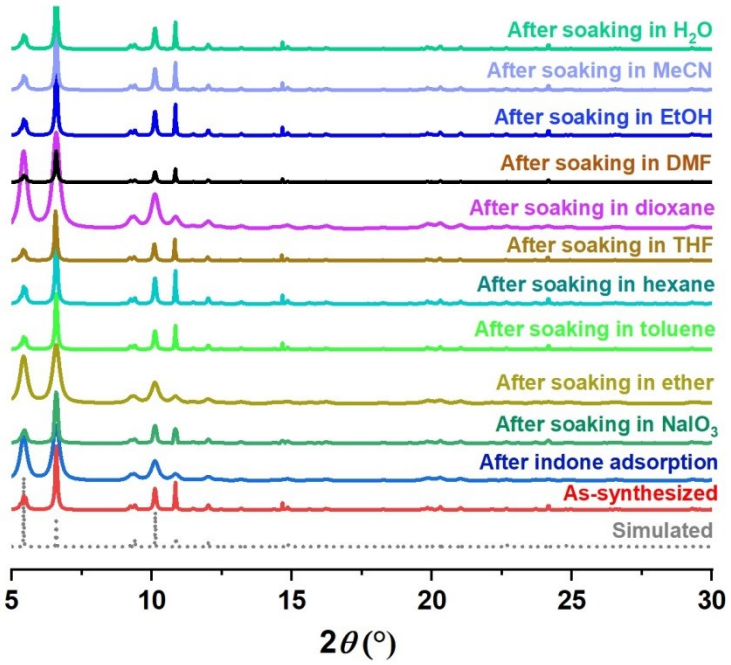

Figure S12. PXRD patterns for compound **1** collected after treatment by soaking in various solutions for 1 day or by fumigation in the iodine vapor atmosphere for 1 day.

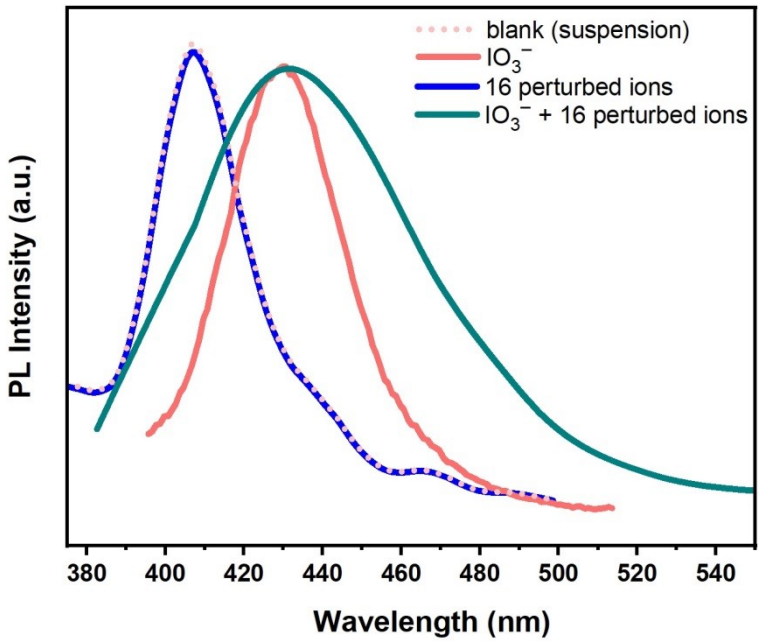

Figure S13. Comparison of photoluminescence spectral changes for suspensions of **1** before (light red dotted line) and after treatment by addition of various ions including lone IO_3^- anion (red line), 16 mixed perturbed ions (Na^+, K^+, Ca^{2+}, Ba^{2+}, Mn^{2+}, Cu^{2+}, Ni^{2+}, Al^{3+}, Ce^{3+} cations, and F^-, Cl^-, Br^-, CO_3^{2-}, HCO_3^-, NO_3^-, SO_3^- anions) (blue line), and IO_3^- anion plus the above 16 mixed perturbed ions (green line) showing the clearly responsive probe effect for IO_3^- anion. Also see legends for each of these.

References

(S1) R. J. Marshall; S. L. Griffin; C. Wilson; R. S. Forgan. Stereoselective halogenation of integral unsaturated C-C bonds in chemically and mechanically robust Zr and Hf MOFs. *Chem. Eur. J*. 2016, **22**, 4870–4877.

(S2) R.-X. Yao; X. Cui; X.-X. Jia; F.-Q. Zhang; X.-M Zhang. A luminescent zinc(II) metal–organic framework (MOF) with conjugated π-electron ligand for high iodine capture and nitro-explosive detection. *Inorg. Chem*. 2016, **55**, 9270–9275.

(S3) D. F. Sava; K. W. Chapman; M. A. Rodriguez; J. A. Greathouse; P. S. Crozier; H. Zhao; P. J. Chupas; T. M. Nenoff. Competitive I_2 sorption by Cu-BTC from humid gas streams. *Chem. Mater*. 2013, **25**, 2591–2596.

(S4) G. Brunet; D. A. Safin; M. Z. Aghaji; K. Robeyns; I. Korobkov; T. K. Woo; M. Murugesu. Stepwise crystallographic visualization of dynamic guest binding in a nanoporous framework. *Chem. Sci*. 2017, **8**, 3171–3177.

(S5) X. Zhang; I. da Silva; H. G. W. Godfrey; S. K. Callear; S. A. Sapchenko; Y. Cheng; I. Vitórica-Yrezábal; M. D. Frogley; G. Cinque; C. C. Tang; C. Giacobbe; C. Dejoie; S. Rudić; A. J. Ramirez-Cuesta; M. A. Denecke; S. Yang; M. Schröder. Confinement of iodine molecules into triple-helical chains within robust metal–organic frameworks. *J. Am. Chem. Soc*. 2017, **139**, 16289–16296.

(S6) Z. Wang; Y. Huang; J. Yang; Y. Li; Q. Zhuang; J Gu. The water-based synthesis of chemically stable Zr-based MOFs using pyridine-containing ligands and their exceptionally high adsorption capacity for iodine. *Dalton Trans*. 2017, **46**, 7412–7420.

(S7) D. F. Sava; M. A. Rodriguez; K. W. Chapman; P. J. Chupas; J. A. Greathouse; P. S. Crozier; T. M Nenoff. Capture of volatile iodine, a gaseous fission product, by zeolitic imidazolate framework-8. *J. Am. Chem. Soc*. 2011, **133**, 12398–12401.

(S8) G. Mehlana; G. Ramon; S. A. Bourne. A 4-fold interpenetrated diamondoid metal-organic framework with large channels exhibiting solvent sorption properties and high iodine capture. *Microporous Mesoporous Mater.* 2016, **231**, 21–30.

(S9) Y. Chen; L. Li; J. Yang; S. Wang; J. Li. Reversible flexible structural changes in multidimensional MOFs by guest molecules (I_2, NH_3) and thermal stimulation. *J. Solid State Chem*. 2015, **226**, 114–119.

(S10) J. He; J. Duan; H. Shi; J. Huang; J. Huang; L. Yu; M. Zeller; A. D. Hunter; Z. Xu. Immobilization of volatile and corrosive iodine monochloride (ICl) and I_2 reagents in a stable metal–organic framework. *Inorg. Chem*. 2014, **53**, 6837–6843.

(S11) G. Massasso; J. Long; J. Haines; S. Devautour-Vinot; G. Maurin; A. Grandjean; B. Onida; B. Donnadieu; J. Larionova; C. Guérin; Y. Guari. Iodine capture by Hofmann-type clathrate $Ni^{II}(pz)[Ni^{II}(CN)_4]$. *Inorg. Chem*. 2014, **53**, 4269–4271.

(S12) Y. Rachuri; K. K. Bisht; E. Suresh. Two-dimensional coordination polymers comprising mixed tripodal ligands for selective colorimetric detection of water and iodine capture. *Cryst. Growth Des.* 2014, **14**, 3300–3308.

(S13) A. Gładysiak; T. N. Nguyen; M. Spodaryk; J.-H. Lee; J. B. Neaton; A. Züttel; K. C. Stylianou. Incarceration of iodine in a pyrene-based metal–organic framework. *Chem.Eur. J*. 2019, **25**, 501–506.

END